Surface Modification of Anodized Titanium Surfaces with Chitosan/ε-Polylysine Coating, Aiming for Improved Bioactivity, Biocompatibility, and Anti-Bacterial Properties for Orthopedic Applications

Dehkordi, Mahshid Jalali ; Bahrami, Abbas; Amin Mokhtari, Mohammad ; Heidari Laybidi, Farnaz ; Roosefid, Ali ; Hosseini-Abari, Afrouzossadat; Yazdan Mehr, M.

Citation (APA)

Important note
To cite this publication, please use the final published version (if applicable).
Please check the document version above.

Article

Surface Modification of Anodized Titanium Surfaces with Chitosan/ε-Polylysine Coating, Aiming for Improved Bioactivity, Biocompatibility, and Anti-Bacterial Properties for Orthopedic Applications

Mahshid Jalali Dehkordi [1], Abbas Bahrami [1], Mohammad Saeid Abbasi [1], Mohammad Amin Mokhtari [1], Farnaz Heidari Laybidi [1], Ali Roosefid [2], Afrouzossadat Hosseini-Abari [2] and Maryam Yazdan Mehr [3,*]

1   Department of Materials Engineering, Isfahan University of Technology, Isfahan 84156-83111, Iran; jalali.m@ma.iut.ac.ir (M.J.D.); a.n.bahrami@iut.ac.ir (A.B.); msaeid.abbasi@gmail.com (M.S.A.); amin.mokhtari1974@gmail.com (M.A.M.); farnazheydari07@gmail.com (F.H.L.)
2   Department of Cell and Molecular Biology & Microbiology, Faculty of Biological Science & Technology, University of Isfahan, Isfahan 81746-73441, Iran; aliroosefid@gmail.com (A.R.); af.hosseini@sci.ui.ac.ir (A.H.-A.)
3   Faculty EEMCS, Delft University of Technology, Mekelweg 4, 2628 CD Delft, The Netherlands
*   Correspondence: m.maryamyazdanmehr@tudelft.nl

Abstract: The increasidng demand for implants due to the aging populations highlights the necessity for applying highly functional coatings on the surface of implants. This study investigates the implications of applying a chitosan/polylysine composite coating on anodized titanium surfaces, aiming for improved biocompatibility, bioactivity, and anti-bacterial properties. Titanium substrates were anodized at 40 volts for a duration of two hours, followed by dip coating with the chitosan/polylysine composite. Fourier-transform infrared (FTIR) analysis was employed to characterize the polymer structure, while field emission scanning electron microscopy (FESEM) and energy-dispersive X-ray spectroscopy (EDS) techniques were utilized to evaluate nanotube morphology and the coating structure. Results showed that samples containing 1.5% polylysine exhibited noticeable anti-bacterial properties and cell viability above fifty percent. Subsequent immersion in simulated body fluid (SBF) for a duration of two weeks revealed the formation of apatite crystals on the coated samples, indicating that the samples are bioactive. Furthermore, polylysine contributed to enhanced resistance against degradation in phosphate-buffered saline (PBS) solution. Overall, the chitosan/polylysine composite coating exhibited promising mechanical and biomedical characteristics, suggesting its potential for applications in orthopedic implants.

Keywords: chitosan; anodizing; titanium; polylysine; biomedical

1. Introduction

Dramatic changes in lifestyle are associated with health challenges, necessitating new approaches and innovative solutions in the biomedical sector [1–3]. With an increase in the average weight and reduced activities, resulting in increasing bone injuries and defects [4]. This clearly necessitates the need for implants and bone graft materials with enhanced properties [5]. Repairing bone defects has always been a challenge, given that infections or immune reactions are always a possibility [6,7]. With that said, there is a demand for safer and more reliable methods to address current bone-related treatments [8,9]. Effective bone regeneration requires perfect attachments, controlled biodegradability, proper nutrient/oxygen transfer, and delivery of vital factors for cell formation and tissue integration [10]. Metallic implants, such as special steel, Co-Cr alloys, and Ti alloys, are widely used options for applications such as joint replacement and fixtures for bone fractures, especially when it comes to applications where high mechanical properties are needed [11].

Ti alloys also demonstrate excellent biocompatibility for orthopedic applications [12]. Nevertheless, the lack of proper bioactivity and the fact that Ti in nature is not anti-bacterial are major concerns in the seamless integration of titanium implants within living tissues [13]. Bacterial infections, associated with implants, have emerged as a difficult and yet very common challenge in the field of orthopedic surgery. To address these concerns, various surface modifications have been proposed, including the inclusion of antibiotics and metal oxides such as Ag, Cu, and Zn on the surface of implants [14]. Using carbon-based materials like carbon nanotubes and graphene, as well as organic coatings such as anti-bacterial peptides, has lately gained attention [15]. While most of these methods are capable of effectively eradicating microorganisms, they may concurrently impose health risks by causing damage in normal cells [16]. With these complications in mind, there is an ever-increasing demand for the development of non-cytotoxic and highly efficient anti-bacterial coatings on biomedical-grade titanium alloys with enhanced bioactivity and osseointegration properties. To this end, cationic antimicrobial peptides have emerged as a promising solution [17]. Antimicrobial peptides have lately been extensively utilized to modify the surfaces of implants, given that they do have superior anti-bacterial characteristics, minimal drug resistance, and low cell toxicity [18]. The incorporation of anti-bacterial peptides into the surface of orthopedic implants appears to be a biologically safe and effective strategy in the creation of anti-bacterial surfaces that are highly resistant against infections while imposing any risk to healthy tissues [19]. Chitosan, a polymer that is derived from partially de-acetylated chitin, is abundantly present in nature, specifically in the exoskeletons of crustaceans and the walls of fungi [20]. The limited solubility of chitosan in physiological solvents, such as water, is attributed to strong intermolecular hydrogen bonding [21]. In acidic aqueous environments (pH < 6), chitosan is positively charged due to the protonation of amino groups, thereby enhancing its solubility by overcoming the associative forces between polymer chains [22]. The anti-bacterial properties of chitosan are ascribed to its polycationic structure, which is essential for electrostatic interactions with the negatively charged bacterial cell wall. The anti-bacterial mechanism, associated with chitosan, involves initial attachment to the cell wall, physical disruption of the cell membrane, attachment to the DNA (thus inhibiting replication), and finally resulting in the cell demise [23]. Protein adsorption, which takes place in the very beginning of implantation, creates a reaction environment in which positively charged amino groups of chitosan electrostatically interact with negatively charged proteins. All these complicated interactions are controlled by factors such as pH, temperature, ionic content of the solution, and the surface properties (i.e., roughness and hydrophobicity) of the biomaterial [24]. The extent of protein adsorption at the surface is a crucial aspect of a biomaterial surface. That and the intricate interactions between the chitosan layer and the adsorbed protein layer are important factors when it comes to the biomedical functioning of the chitosan-coated implant [25]. When it comes to properties of a novel composition or coating in biomedical applications, it is of crucial importance to evaluate different structural aspects and biological interactions of the material with the surrounding tissue [26–28].

ε-Polylysine (ε-PL) is a biopolymer naturally produced by Streptomyces albulus, attracting loads of attention from the biomedical community in recent years. ε-PL is known to have remarkable anti-bacterial properties and superior biocompatibility. Also, noticeable water solubility and temperature resistance are reported in this polymer [29]. These properties make ε-PL a promising candidate for biomedical applications. The anti-bacterial effectiveness of ε-PL can be related to electrostatic interactions between the positively charged amino ($-NH^{3+}$) groups in the polylysine structure and the surfaces of microorganisms [30]. This type of interaction results in the destruction of cell membranes of microorganisms [31]. The anti-bacterial effectiveness of polylysine essentially has to do with the quantity of protonated NH^{3+} groups or the presence of L-lysine residues in its structure [32]. It is postulated that there is a positive association between the molecular weight of polylysine and its anti-bacterial properties [32]. Larger molecular weights are believed to be associated with enhanced anti-bacterial efficacy, resulting in a decrease in

the minimum inhibitory concentration of *S. aureus* [33]. Currently, ε-PL and its derivatives have shown very promising results in cancer treatment due to their exceptional stability and efficiency in drug encapsulation [34]. Additionally, ε-PL plays a vital role in tissue adhesion [34] and the healing of bacteria-infected wounds [35]. The diverse range of applications for ε-PL highlights its potential importance in various biomedical applications and makes it one of the most promising biopolymers when it comes to the coating of implants.

This study investigates the effects of surface modification of anodized titanium using innovative chitosan/polylysine composite coatings, aimed at improving the properties of pure titanium for biomedical applications. Titanium alloy substrates underwent anodization to generate nanotubular structures on their surfaces, enhancing their functional properties. Following the anodization process, various polymeric compositions of chitosan and polylysine were applied to the modified titanium surfaces. The primary focus of this research was to assess the anti-bacterial and biomedical performance of chitosan/polylysine-modified titanium alloys. The novelty of this study lies in the application of composite coatings, which provide an effective approach to enhancing the bioactivity, anti-bacterial properties, and overall performance of pure titanium, making it more suitable for use in medical implants.

## 2. Materials and Methods

2.1. Materials

Ammonium fluoride (NH_4F, Sigma-Aldrich, Darmstadt, Germany), Chitosan (190 KDa, Sigma-Aldrich, Darmstadt, Germany), phosphoric acid (H_3PO_4, Sigma-Aldrich, Darmstadt, Germany), and Poly-ε-Lysine (ε-PL, Sigma-Aldrich, Darmstadt, Germany) were used to prepare the anodized bath.

2.2. Sample Preparation

To attain nanotubes over the surface of substrates, an anodizing solution was prepared by mixing 100 mL of distilled water with phosphoric acid. Then, 0.37 g of NH_4F. A polymeric solution was prepared by adding 10 g per liter of chitosan, combined with 1 volume percentage of acetic acid, in a solvent volume of 10 mL of water. Chitosan-0.5% ε-PL, chitosan-1% ε-PL, chitosan-1.5% ε-PL, and chitosan-3% ε-PL samples were prepared by adding the proper amount of ε-PL to the chitosan solution. Polymeric coatings were applied by the dip-coating method. A substrate made of Ti_6Al_4V, cut in 10 $\times$ 30 mm, was used in this study. The anodizing procedure for the substrate was carried out for 2 h at a potential difference of 40 V. Samples were heated at 550 °C to facilitate the formation of the anatase phase. Anodized samples were cleaned with ultra-solicitation for 30 s before coating chitosan/ε-PL coating layers. The dip-coating technique was chosen on the grounds that it provides a uniform coating layer over surfaces. Coated samples were left to air-dry at ambient temperature for 48 h. The schematics of the sample preparation are shown in Figure 1.

2.3. Materials Characterizations

A series of tests were conducted to comprehensively characterize the samples and coatings under investigation. The analytical techniques employed provided insights into the structural, chemical, and physical properties of the materials, as well as their biological and anti-bacterial performance. FTIR was performed to determine the structure and chemical composition of the coatings; SEM (SEM, Philips 30 Xl, Eindhoven, The Netherlands) and energy dispersive X-ray spectroscopy (EDS) were performed to investigate the surface structure and chemical composition of coatings, respectively. The contact angle was measured to assess the hydrophobicity of the surface. The surface roughness and the topography of the coating layer were evaluated using a laser profilometer. And finally, biological tests were performed to check the bioactivity and biocompatibility of the coatings, and anti-microbial tests were conducted to evaluate the anti-bacterial properties of ε-PL-chitosan coatings.
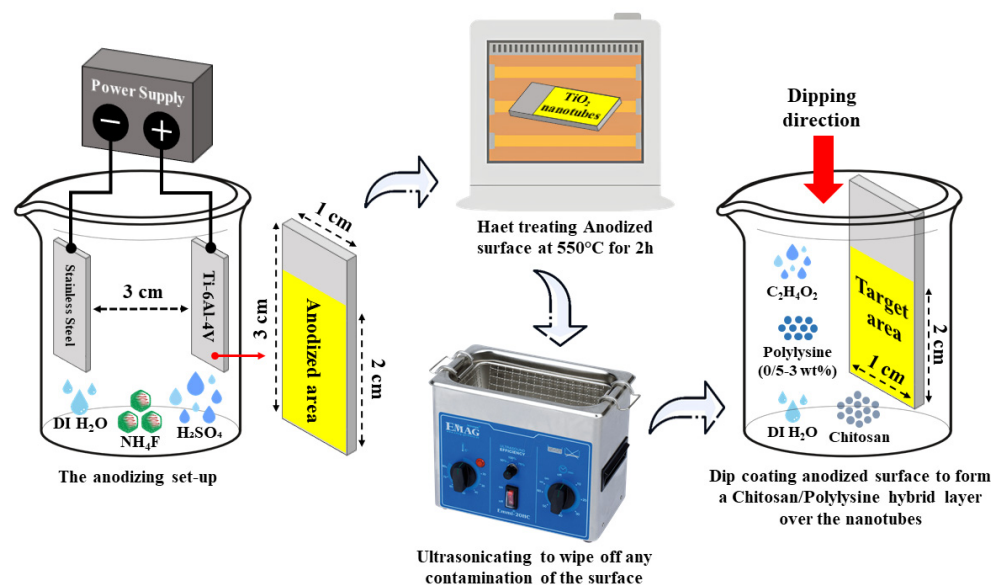
Figure 1. Schematic representation of the experimental procedure for fabricating and modifying the Ti-6Al-4V anodized surface. The process includes anodizing in an electrolyte solution, heat treatment at 550 °C for 2 h, ultrasonic cleaning to remove contaminants, and subsequent dip-coating in a chitosan/polylysine solution to form a hybrid layer over the nanotubes.

2.4. Biological Characterizations

To evaluate the bioactivity of coated samples, samples were exposed to simulated body fluid (SBF) solution (1X concentration, $142Na^+$-$5K^+$-$1.5Mg^{2+}$-$2.5Ca^{2+}$-$148Cl^{-1}$-$4.2HCO_3$—$1HPO_4^{3-}$-SO_4^{2-}), for two weeks to monitor the formation of hydroxyapatite crystals, expected to be formed by the release of P and Ca ions from the solution. The temperature was kept constant at 37 °C in a water bath during the test. During the 14-day immersion period, the pH of the solution was monitored every day. The formation of hydroxyapatite on samples was investigated utilizing SEM, enabling detailed visualization of the precipitated crystals. Furthermore, the contents of Ca and P present in the solution were quantitatively analyzed by the application of inductively coupled plasma mass spectrometry (ICP). This multi-faceted approach provided comprehensive insights into the bioactivity and efficacy of the coated samples in facilitating the precipitation of hydroxyapatite crystals, a crucial indicator of their potential for biomedical applications. To conduct in-vitro bioactivity tests, representative Gram-positive bacteria (*Staphylococcus aureus ATCC 6538*) and Gram-negative bacteria (*Escherichia coli ATCC10536*) were used with a 0.5 McFarland concentration to attain a standard bacterial suspension for consistent testing conditions. Afterwards, bacterial suspensions were incubated at 37 ± 2 °C for 24 h. The controlled incubation period allows for the assessment of bacterial growth under optimal conditions. Following the incubation period, each sample underwent dilution, down to 10^{-6} to 10^{-1}. These dilutions were accurately prepared to create a range of concentrations for thorough testing and analysis. Subsequently, diluted samples were cultured for an extra 24 h at 37 ± 2 °C. After the incubation period, the count of colonies at each concentration was conducted. This step enables the quantification of bacterial growth under varying concentrations and conditions. Finally, the colony counting was carried out. Deviations from the control sample provide valuable insights into the anti-bacterial response of tested substances against the chosen bacteria, helping to evaluate their usefulness and prospects for further anti-bacterial applications.

Biocompatibility/cell viability of specimens was evaluated by the MTT (3-(4,5-dimethylthiazol-2-yl)-2,5-diphenyltetrazolium bromide) assay, according to the ISO 10993-5:2009 standard [36], which is basically based on the gauging of the viability of cells by evaluating the variation in MTT color within the mitochondria of living cells. MTT is a photometric estimate of viable cell numbers. Before the MTT test, specimens were sterilized

in an autoclave. The MTT test involved seeding 1×10^4 MG63 cell samples with DMEM culture media into 96-well plates in triplicate. Various contents (100, 50, 10, 5, and 1%) and 10 μM of the sample solution were poured into the wells three times and incubated in a 5% carbon dioxide atmosphere at 37 ± 1 degrees Celsius for 24 h. Following this treatment, each well received 20 microliters of 5 mg/mL MTT dye. More details on the MTT protocol can be found here [13].

3. Result and Discussion

3.1. FTIR-ATR Analysis

Figure 2 represents the ATR-FTIR results from chitosan, ε-PL, and chitosan-ε-PL coatings on anodized Ti_6Al_4V substrate. The presence of discernible FTIR peaks approves the complete coatings of these polymers onto the substrates, with identifiable peaks related to typical vibrational modes of both chitosan and ε-PL. The ATR data clearly elucidate the chemical structure of the deposited layers, displaying well-known peaks linked to functional groups in both chitosan and ε-PL. Chitosan is a natural polysaccharide with a chemical formula ($C_8H_{13}NO_5$), and amino groups in ε-PL are clearly present, providing strong evidence of the active deposition of these polymers over the surface. The mixture of these coatings is predicted to end up in a change in peak height, as depicted in Figure 2. Particularly in the case of chitosan, the strongest peak is at 3250, while the weakest one is centered at 600. In the case of ε-PL, these peaks are seen at 1617 and 1047, respectively.
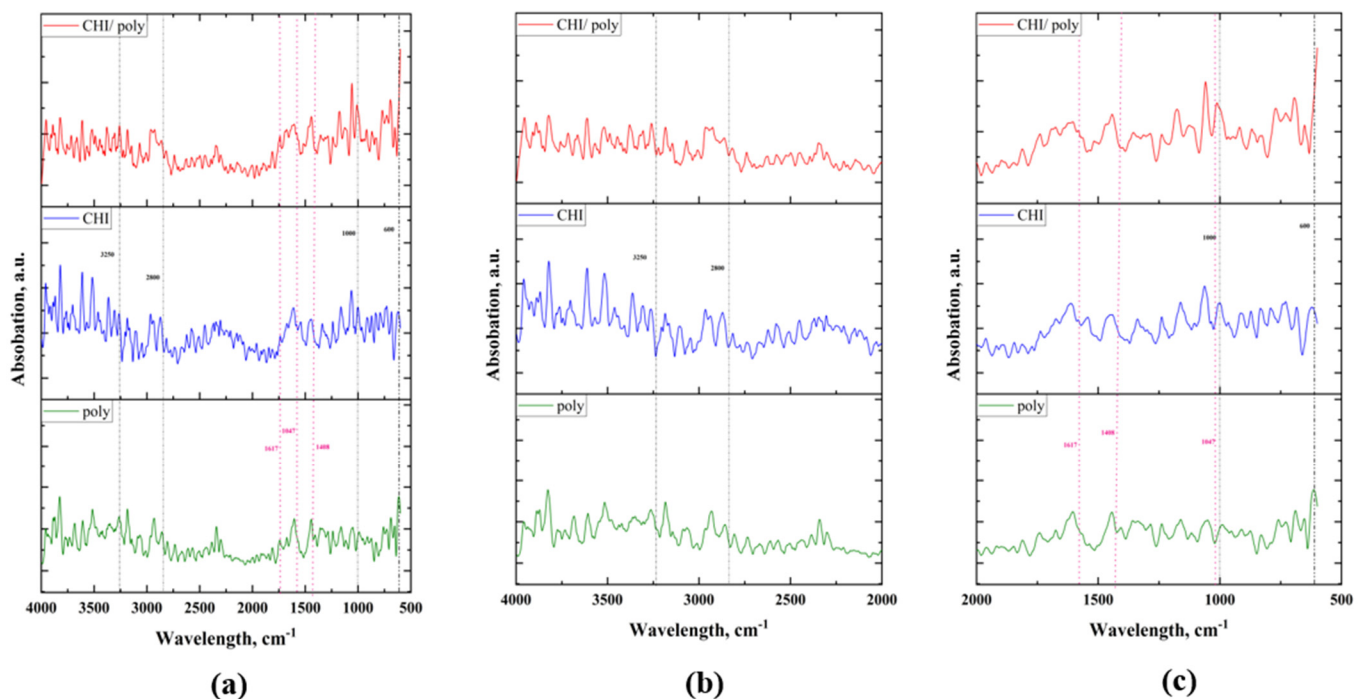

Figure 2. ATR-FTIR for chitosan, ε-PL, and chitosan-ε-PL samples at (**a**) 500 to 4000, (**b**) 2000 to 4000, and (**c**) 500 to 2000 cm^{-1}.

3.2. Stereomicroscope Results

Stereomicroscope images of an uncoated anodized sample and those of specimens coated with chitosan-x%ε-PL ($0.5 < x < 3$%) are shown in Figure 3. Figure 3a shows the uncoated surface, entirely in yellow. Subsequently, Figure 3b depicts the coated surface with pure chitosan (in purple), which exhibits complete uniformity all over the surface. Figure 3c illustrates the impact of introducing ε-PL into the chitosan matrix. It is evident that the addition of ε-PL has some implications for the coating layer. As the concentration of ε-PL in the coating increases, the topology of the coating layer changes in such a way that some uncoated yellowish spots are visible over the surface. This phenomenon is

likely due to the change in the shrinking behavior caused by the addition of ε-PL to the chitosan matrix.
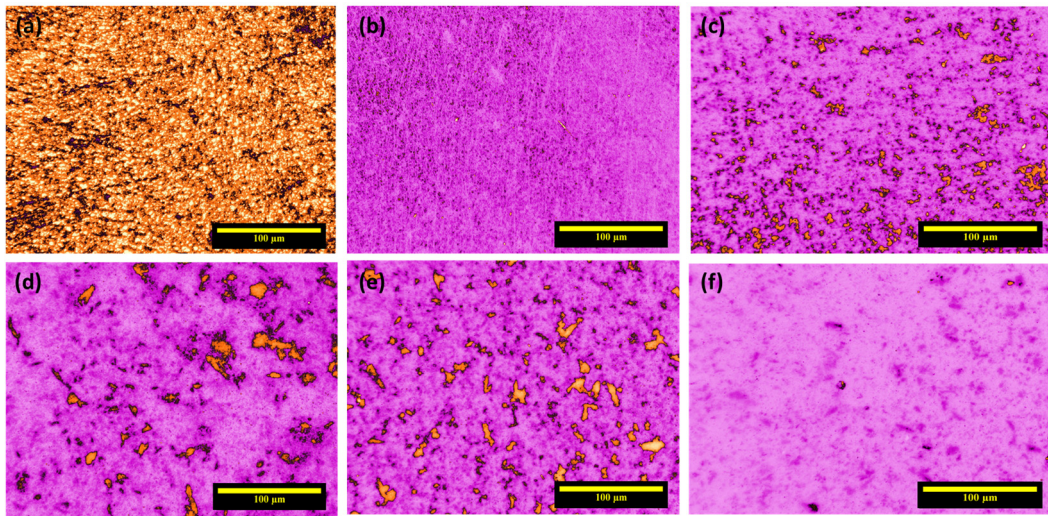
Figure 3. Stereomicroscope micrographs of (**a**) as-received Ti_6Al_4V surface and surfaces with (**b**) chitosan, (**c**) chitosan-0.5% ε-PL, (**d**) chitosan-1.0% ε-PL, (**e**) chitosan-1.5% ε-PL, and (**f**) chitosan-3.0% ε-PL as coating layers.

3.3. FE-SEM Microscopy

Figure 4 illustrates FE-SEM images of TiO_2 nanotubes formed on the anodized surface together with EDS analysis. As expected, the EDS/SEM results show titanium and oxygen-related peaks, inferring that TiO_2 nanotubes have been successfully attained and that the grown nanotubes are closely packed with hardly any space in-between. Also, it is noticeable that the TiO_2 nanotubes have a relatively uniform diameter, implying that they have a uniform distribution over the surface.
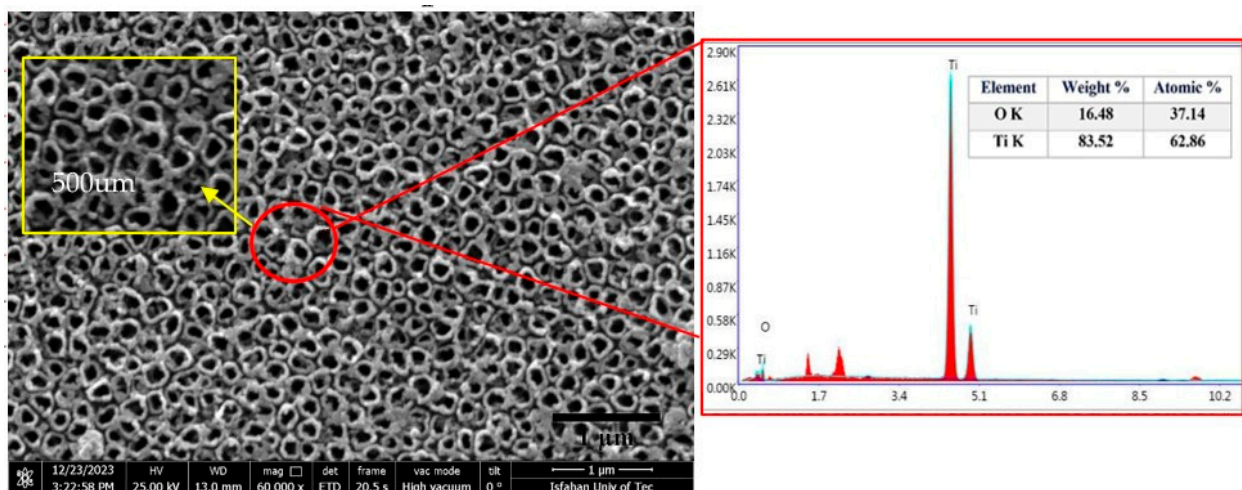
Figure 4. FE-SEM/EDS analysis of TiO_2 nanotubes over anodized surface.

Figure 5 shows SEM images from the surface of anodized titanium coated with the chitosan and ε-PL-containing chitosan composites. It can be seen that in all compositions, the surface is fully covered with the polymeric coating layer. The most noticeable feature in these coatings is the presence of some white spots in the coating layer, and the number of these rough white surface spots varies with the composition. As can be seen, the surface roughness decreases with increasing the content of ε-PL in the coating composition up to

1% ε-PL, followed by a slight increase in the roughness in samples containing higher ε-PL. It appears that the sample chitosan-1.0% ε-PL has the highest uniformity and smoothness among all samples. Also, EDS analyses/elemental mapping in Figure 6 show the presence of peaks related to titanium, silicon, magnesium, phosphorus, aluminum, carbon, and oxygen in all samples, coming from the substrate and the coating layer. It is noteworthy that in all cases, there is a homogeneous dispersion of alloying elements in coating layers.
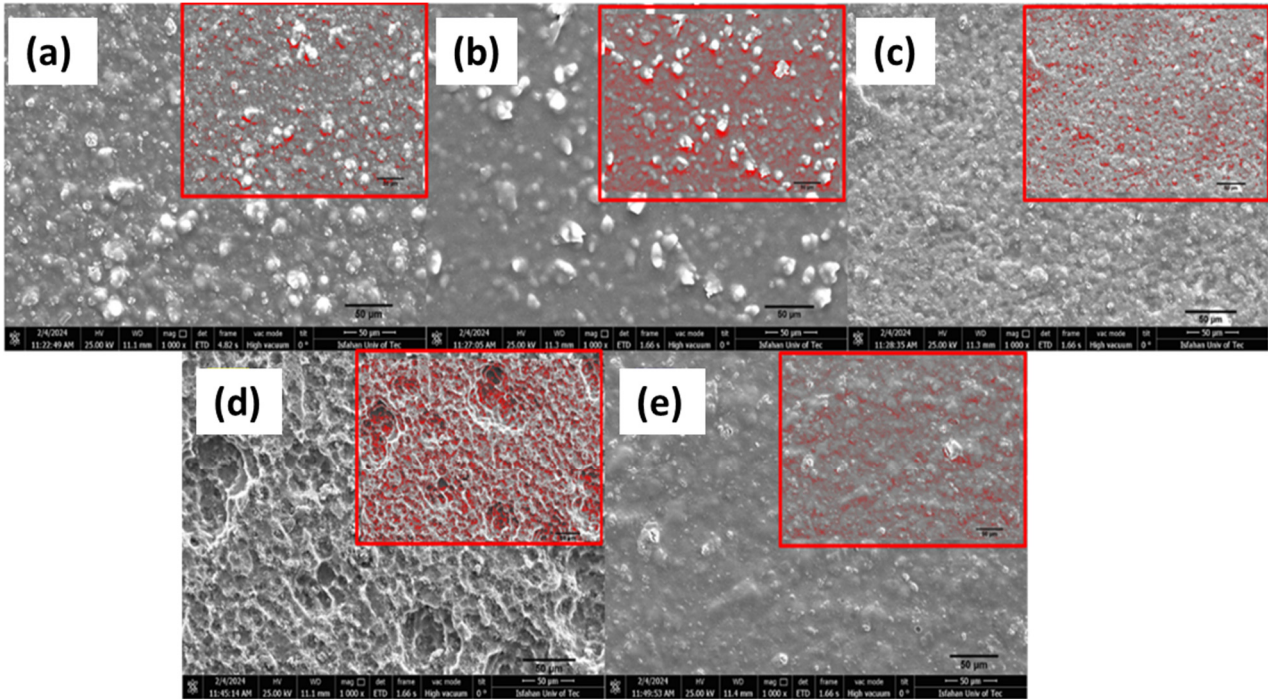
Figure 5. FE-SEM images for (**a**) chitosan coating, (**b**) chitosan-0.5% ε-PL, (**c**) chitosan-1.0% ε-PL, (**d**) chitosan-1.5% ε-PL, and (**e**) chitosan-3.0% ε-PL. all with a scale bar of 50 μm.

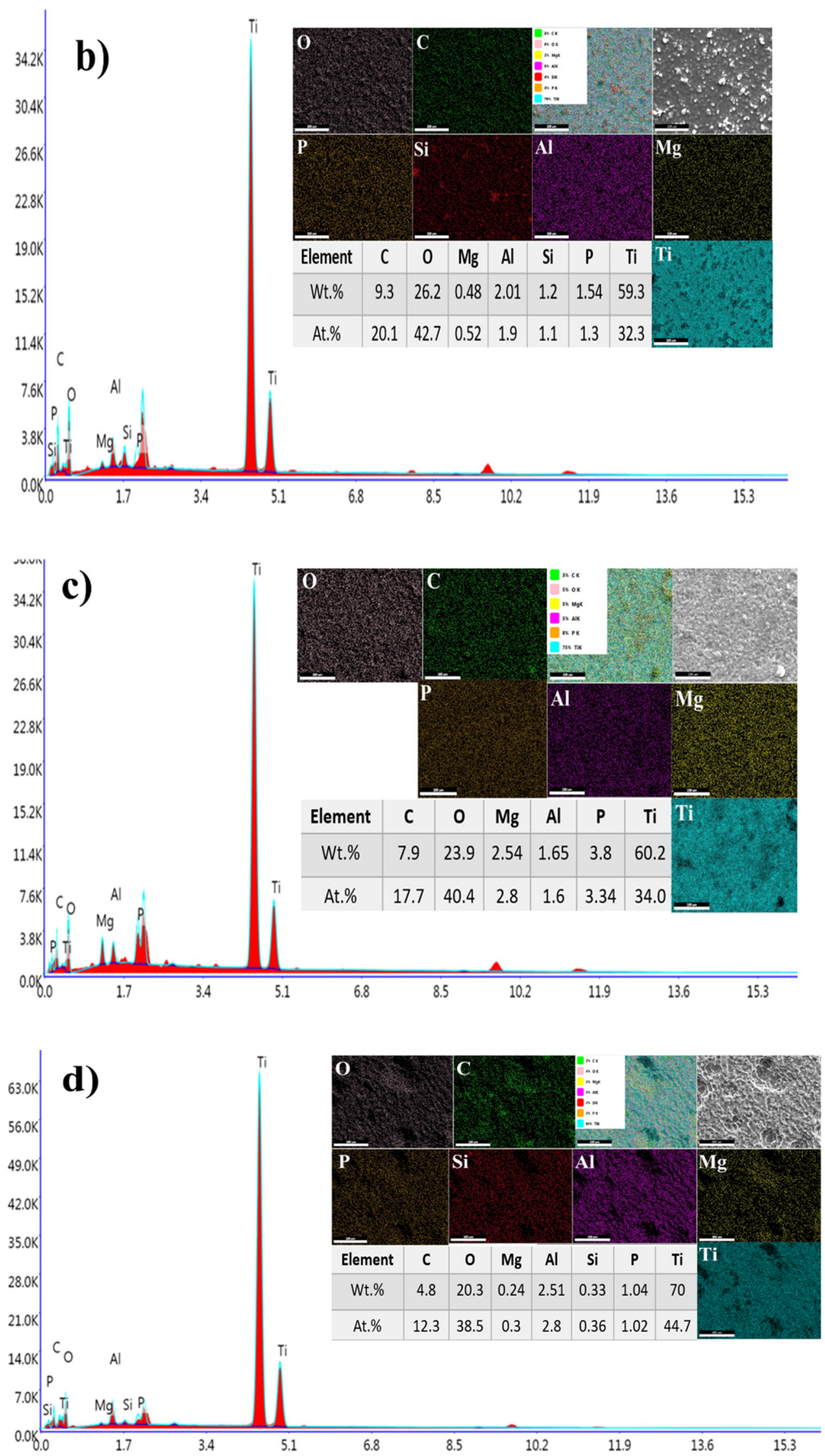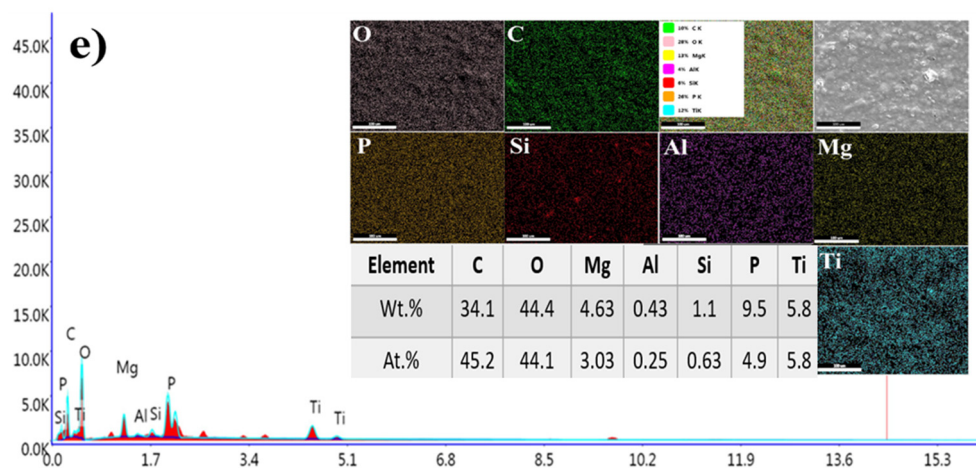| Element	C	O	Mg	Al	Si	P	Ti
Wt.%	23.7	37.7	1.8	0.9	0.5	4.8	30.6
At.%	37.6	44.9	1.4	0.6	0.3	2.9	12.1
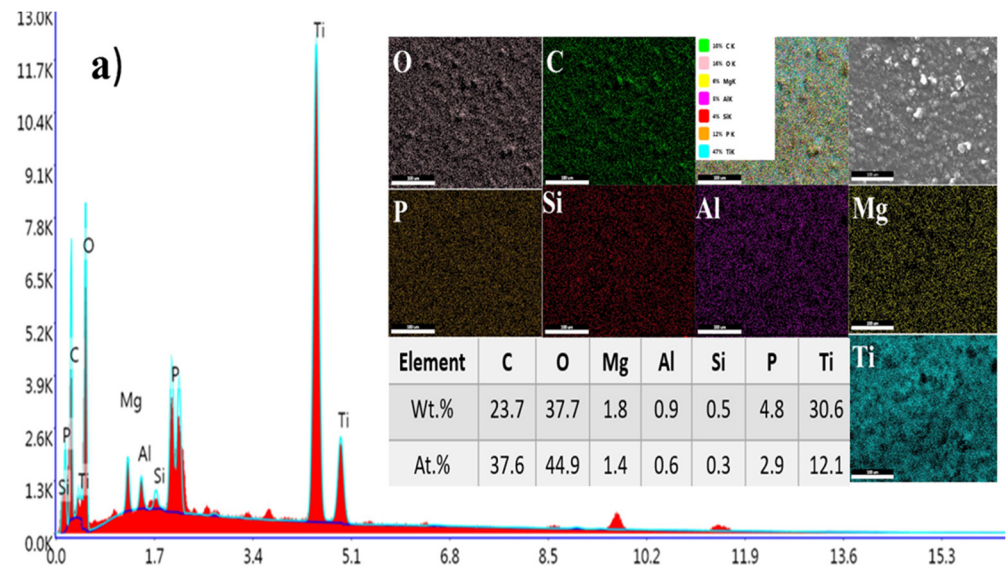
Figure 6. *Cont.*

Figure 6. *Cont.*

Figure 6. EDS analyses/elemental mapping for (**a**) chitosan layer, (**b**) chitosan-0.5% ε-PL, (**c**) chitosan-1.0% ε-PL, (**d**) chitosan-1.5% ε-PL, and (**e**) chitosan-3.0% ε-PL. all with a scale bar of 100 μm.

3.4. Contact Angle Measurements

Wettability is certainly an important surface characteristic, not only in biomedical applications but also in surface-related applications [37–39]. Wettability analyses performed on surfaces with and without coating shown in Figure 7. According to the theory and as confirmed by the presented, it is expected that the hydrophilicity of Ti samples will increase when samples are anodized. This has to do with the increased surface area due to the formation of nanotubes on the surface. The hydrophobicity of the chitosan-coated surface is comparatively much higher than that of the anodized surface, resulting in contact angles as high as 100 degrees. The addition of ε-PL to the chitosan matrix is associated with a significant decrease in contact angles, rendering more hydrophilic surfaces, which is certainly a positive attribution. The lowest contact angle (60°) was attained in the chitosan-1.5% ε-PL sample. Further increase in the ε-PL content of the coating layer up to 3.0% ε-PL is accompanied by a slight increase of the wetting angle, inferring that the chitosan-1.5% ε-PL coating has the highest hydrophilicity. The fact that the presence of the ε-PL in the chitosan matrix results in a lower contact angle suggests that the number of n-acetyl-glucosamine groups in the coating structure has increased. These amino groups are expected to establish hydrogen bonds with hydroxyl groups. Consequently, the formation of hydrogen bonds and enhanced molecular bonding between polylysine-covered chitosan and surrounding surfaces possibly contribute to the observed reductions in the contact angle, thereby modifying the surface properties of the coating. This observed increase in the hydrophilicity of the coating is expected to enhance the biological properties and bioactivity of the surface [12,13].

In terms of morphology, ε-PL concentration affects the surface structure of the composite coatings. At 1%, the polymer distribution is insufficient, resulting in simpler and less refined surface features. At 1.5%, optimal interactions between ε-PL and the chitosan matrix produce a smoother, more uniform morphology, enhancing hydrophilicity. In contrast, at 3% ε-PL, excessive polymer disrupts surface uniformity through aggregation or microphase separation, leading to rougher surface features and diminished hydrophilic behavior. These findings highlight the critical role of optimizing ε-PL concentration to achieve desirable surface properties. Notably, all p-values for the variables presented in Figure 7 were below 0.05 ($p < 0.05$).
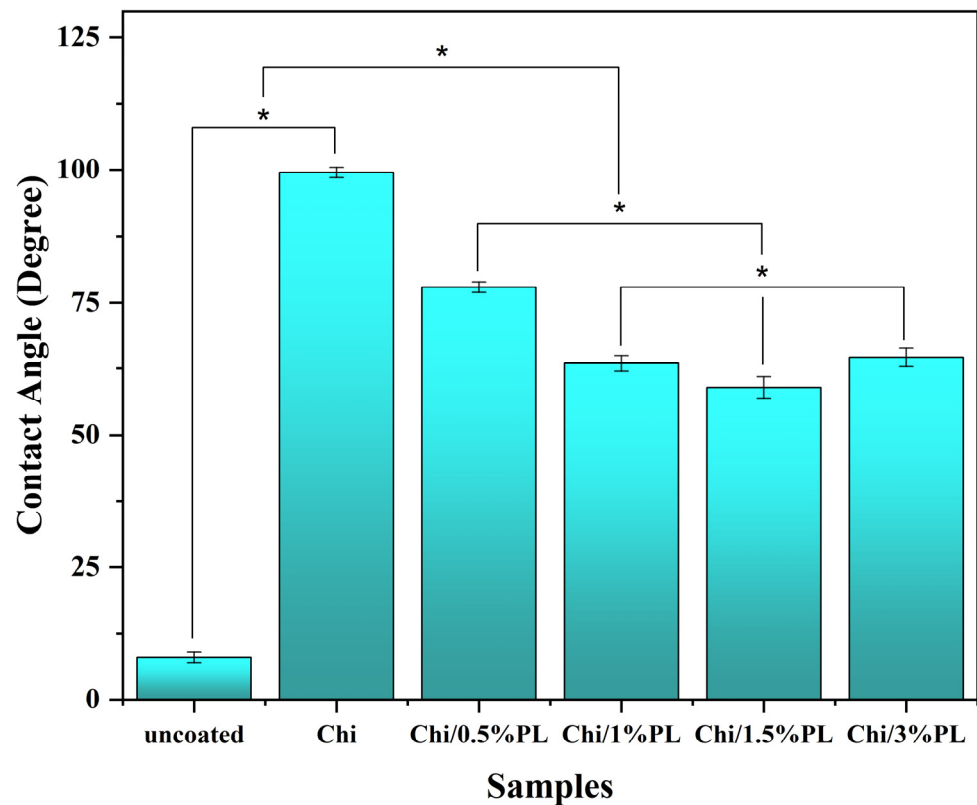
Figure 7. The result of contact angle measurements for anodized Ti_6Al_4V surface and surfaces, coated with chitosan-x% ε-PL (0.5 < x < 3.0%) layer. (*: $p < 0.05$, The data underwent analysis through a one-way ANOVA method, followed by Tukey's post-hoc test for further evaluation. Statistical significance was established at a threshold of $p < 0.05$ to identify any meaningful differences).

3.5. Surface Roughness Evaluations

A roughness test (laser profilometry) was first conducted on the anodized surface. The growth behavior of nanotubes on the Ti_6Al_4V substrate, containing both alpha and beta phases, presents distinct characteristics for each phase. In the alpha phase, the resulting nanotubes display a lower thickness coupled with an increased height. On the contrary, the beta phase exhibits nanotubes with increased wall thickness and reduced height [40–42]. Figure 8 depicts the surface topography of coated specimens with different contents of polylysine. The chitosan-coated surface has a clearly different topography as compared with those containing ε-PL additive. The chitosan coating layer has a comparatively coarser surface topography with deeper valleys. It appears that the presence of ε-PL in the chitosan layer has resulted in finer surface topography, possibly because ε-PL has led to a smoother and easier distribution of the coating layer over the surface. This is shown in numbers in Figure 9, where a dramatic decrease in the surface roughness has taken place when ε-PL is added to the chitosan matrix.

Based on the results of surface roughness and contact angle measurements, the sample containing 1.5% ε-PL was considered the optimal sample for further investigation. It appears that this particular composition has favorable characteristics in terms of wetting angle and hydrophilicity, making it a potentially optimal choice for the intended application.
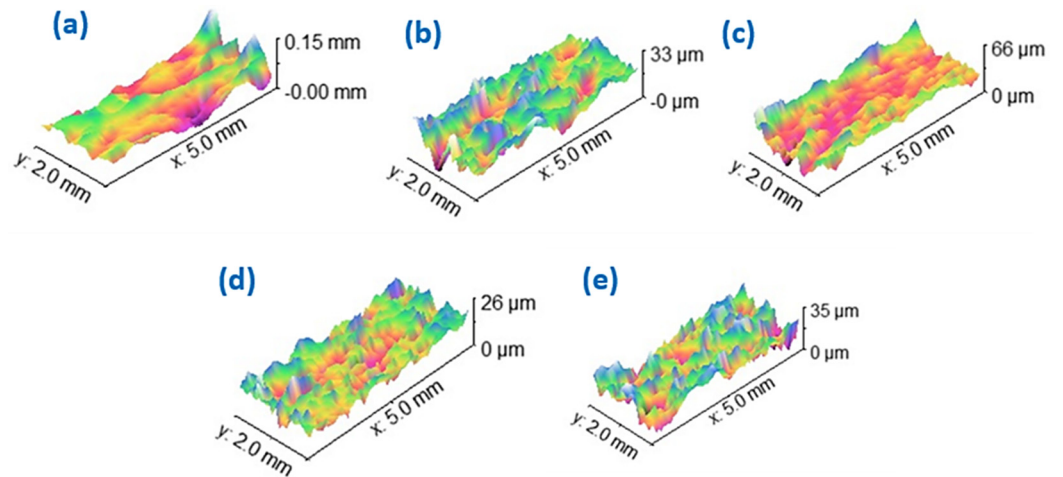
Figure 8. Surface profilometry for (**a**) chitosan layer, (**b**) chitosan-0.5% ε-PL, (**c**) chitosan-1% ε-PL, (**d**) chitosan-1.5% ε-PL, and (**e**) chitosan-3% ε-PL.
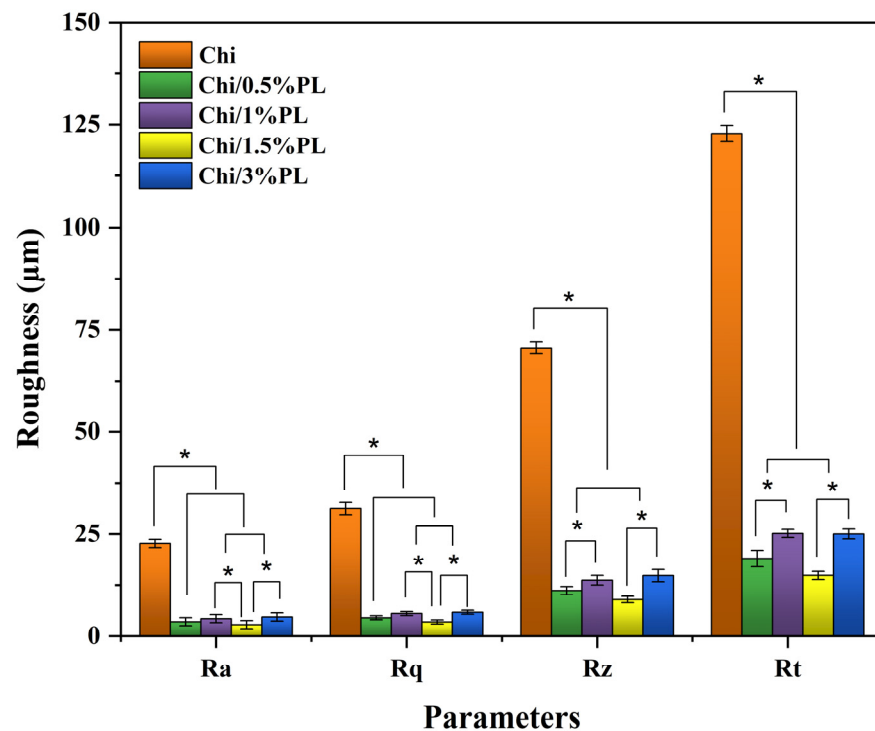

Figure 9. Surface roughness for ε-PL-containing chitosan coating layers. (*: $p < 0.05$, notably, all *p*-values for the variables presented in Figure 9 were below 0.05 ($p < 0.05$)).

3.6. MTT Test Results

After a period of 24 ± 2 h, the MTT tests on the sample chitosan-1.5% ε-PL were conducted at 5 different concentrations (100%, 50%, 10%, 5%, and 1%) with three repetitions for each concentration (results are shown in Figure 10). Evaluation of cell activity was performed visually. In order to make sure the MTT test has been conducted properly, the control sample is expected to exhibit 100% cell viability, as expected. To ensure that data are repeatable, the standard deviation was fixed at less than 15% to make sure that results are reliable. The survival percentage in each sample was compared with that of the control sample, indicating the cytotoxicity of the chitosan-1.5% ε-PL sample. A test sample is considered non-cytotoxic in case viability exceeds 70%. Otherwise, it is classified as a cytotoxic substance. The percentage of cell survival near the sample, measured at five different concentrations with 3 replicates for 2 h, showed hardly any cytotoxicity

at concentrations below 50 μM. Higher contents of ε-PL might be considered relatively toxic. At concentrations exceeding 50 μM, polylysine exhibits cytotoxicity due to its strong electrostatic interactions with cell membranes and intracellular molecules. Its highly cationic nature disrupts the integrity of cell membranes, increasing permeability and leading to cell lysis. Additionally, elevated concentrations of polylysine induce oxidative stress through reactive oxygen species (ROS) generation, causing damage to lipids, proteins, and DNA, which reduces cell viability and triggers apoptosis. Polylysine can also interfere with essential cellular processes, such as protein synthesis and DNA replication, through its binding to nucleic acids and proteins. High intracellular uptake via endocytosis disturbs cellular pH, osmotic balance, and organelle function. Aggregation on the cell surface at toxic concentrations may further block nutrient and gas exchange while proinflammatory responses amplify its cytotoxic effects. These combined mechanisms highlight the dose-dependent nature of polylysine toxicity [43–45].
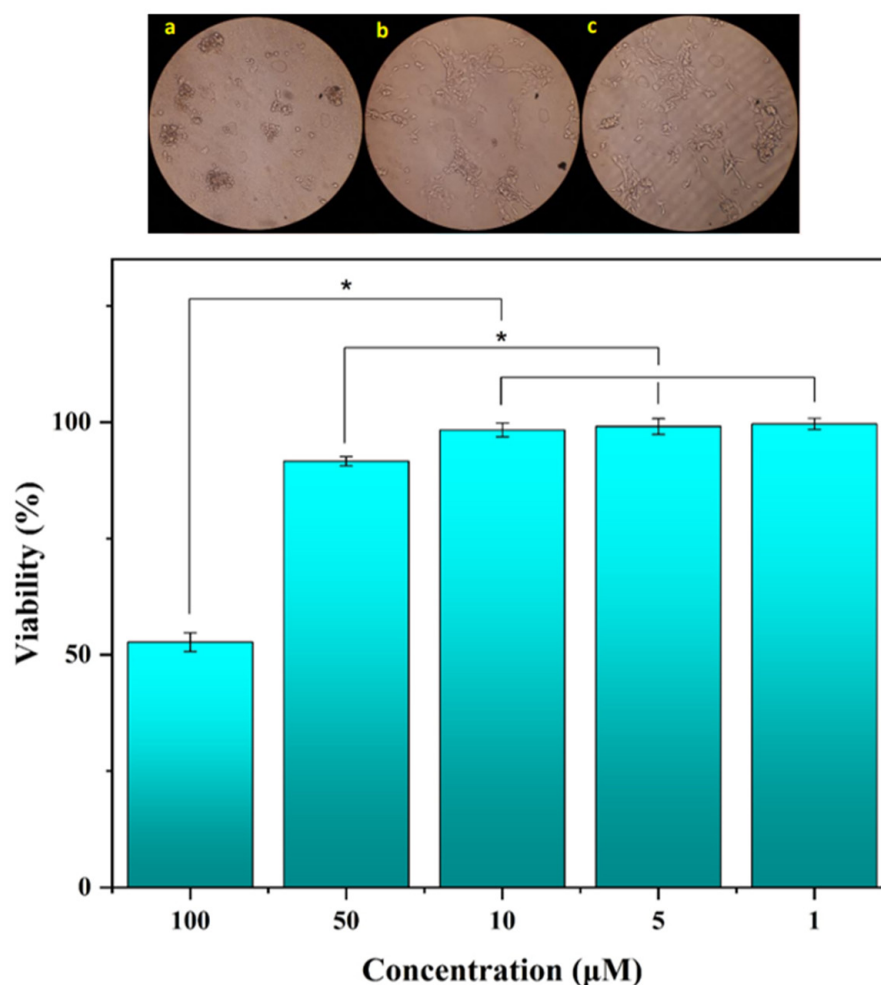

Figure 10. The results and images of cell viability tests after a period of 24 ± 2 h: (**a**) concentrations 1 μM, (**b**) 100 μM, and (**c**) control sample. (*: $p < 0.05$, notably, all *p*-values for the variables presented in Figure 10 were below 0.05 ($p < 0.05$)).

3.7. Anti-Bacterial Evaluations

The process of bacterial cell counting is a routine biological procedure used to determine the concentration of bacterial cells within a culture medium. It starts with cultivating a set volume of cells in a culture medium. By counting individual colonies, cell concentrations can be estimated relatively accurately. In this investigation, the colony count method was used to evaluate the anti-bacterial efficacy against two widely used bacterial types: *E. coli* and *Staphylococcus*. The anti-bacterial responses of samples coated with chitosan and

chitosan-1.5%ε-PL were investigated. Results indicated a noticeable decrease in bacterial activity in both chitosan and chitosan-1.5%ε-PL samples. In the case of *Staphylococcus aureus*, the number of bacteria was dropped by 10.5×10^8 and 12×10^8 CFU/mL in chitosan and chitosan-1.5%ε-PL samples, showing a comparatively better performance when ε-PL is used as an additive. In the case of *E. coli*, no meaningful difference was observed, where both samples showed a reduction in the number of colonies in the order of 63×10^8 CFU/mL. Figure 11 gives a visual overview of the colony count test. Overall, it appears that the anti-bacterial contribution of ε-PL addition is marginal.
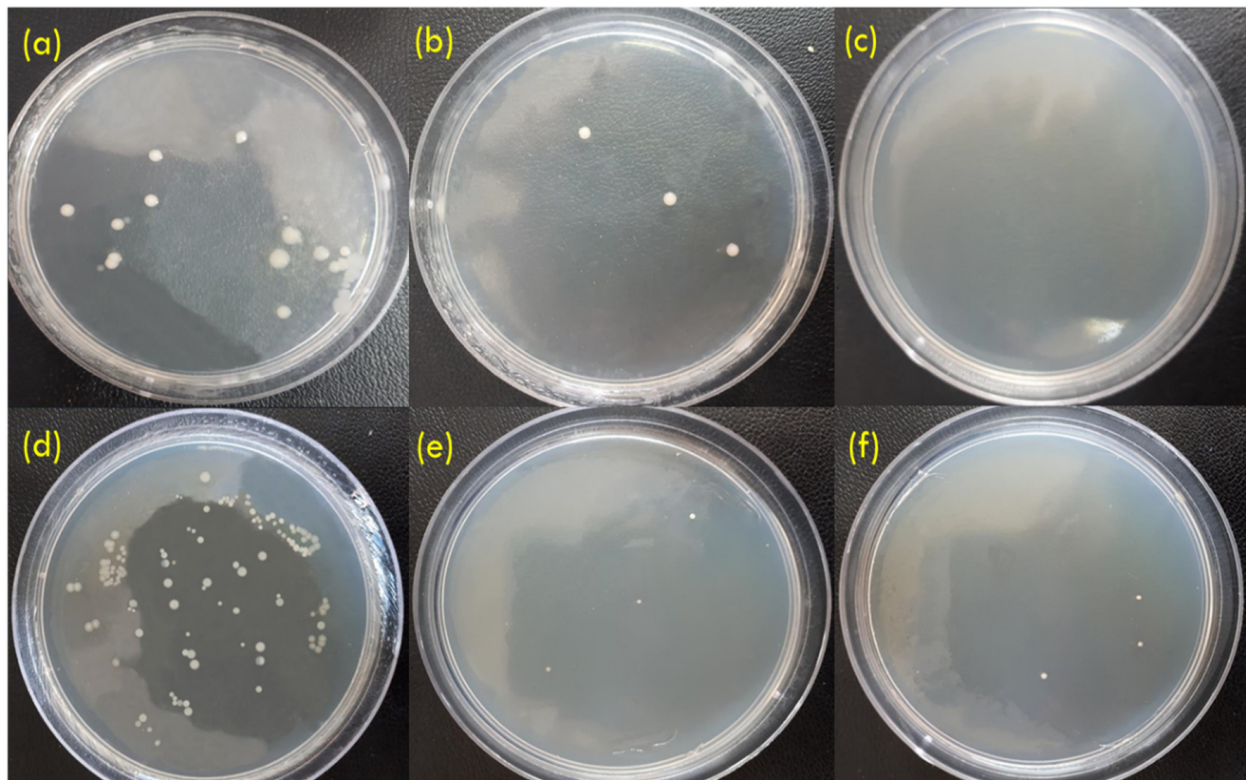
Figure 11. Results of colony count test for (**a**) control sample, (**b**) chitosan, (**c**) chitosan-1.5% ε-PL with colony counts of 24, 3, and 0, respectively, against *Staphylococcus aureus*, (**d**) control sample, (**e**) chitosan, and (**f**) chitosan-1.5% ε-PL with colony numbers of 130, 3, and 3 against *E. coli*.

3.8. ICP Test/pH Measurements

Figure 12 shows results of monitoring pH and Ca/P concentrations in simulated body fluid (SBF) solution for coated samples with chitosan and chitosan-ε-PL composite coatings during a 2-week immersion test. As depicted in Figure 12a, changing the pH of the solution has an initial decreasing trend down to a minimum, followed by a rather sharp increase to values close to 7. While the initial decrease has possibly to do with the partial dissolution of the chitosan layer, the following increase is likely due to the competing hydroxyapatite crystal formation/dissolution reactions over the surface. The formation of apatite crystals on the surface can be confirmed by decreasing the content of Ca and P ions in the solution, which is clearly visible in Figure 12b. As observed in this figure, the early contents of P and Ca in the SBF solution are measured as 47 and 50 mg/dL, correspondingly. All specimens showed a considerable decrease in the content of P and Ca when compared to the initial solution, implying a depletion of these elements from the solution.
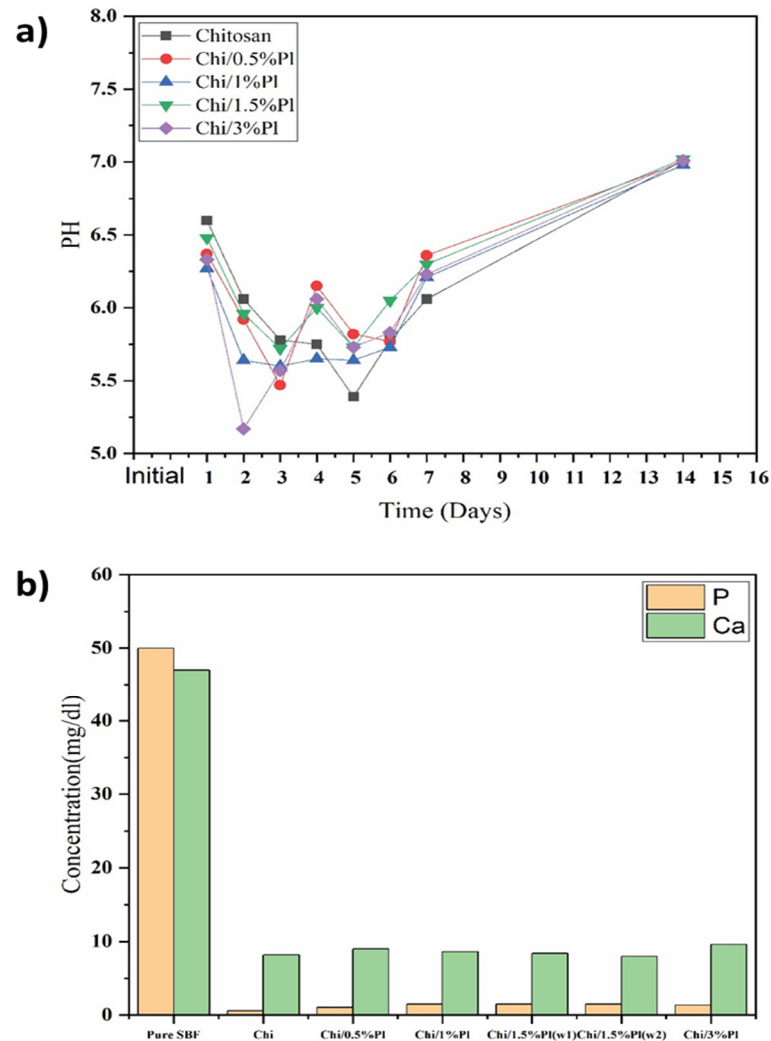
Figure 12. (**a**) The changes in the pH of the solutions in this period of immersion in the SBF solution and (**b**) variations in the phosphorus and calcium in the SBF solution, as compared with the as-received SBF solution.

3.9. Bioactivity Test

The bioactivity of various composite layers was investigated by checking the formation of hydroxyapatite (HA) crystals over the surface of the specimens. The outcomes for samples chitosan, chitosan-1.5% ε-PL, and chitosan-3.0% ε-PL are presented in Figure 13. The specimens were immersed in 15 mL of SBF solution in a water bath at 37 °C for up to fourteen days. As the Ca and P contents in the SBF solution decrease (as shown in Figure 12b), as anticipated, hydroxyapatite crystals will form on the surface of the specimens, which can be taken as an indication of bioactivity. The formation of hydroxyapatite crystals was confirmed through scanning electron microscope and EDS analyses. The results showed that in all cases there is Ca and P in the composition of precipitated phases, confirming the aforementioned argument on the precipitation of P and Ca from the SBF solution, accompanied with the precipitation of the HA phase. Yet, the fact that the Ca/P ratio is relatively low in all cases implies that applied coatings do not have high bioactivity. At the same time, results indicate that the presence of ε-PL in the chitosan matrix is associated with some alterations in the morphology of precipitated phases over the surface, with the finest surface features seen in sample chitosan-1.5% ε-PL.
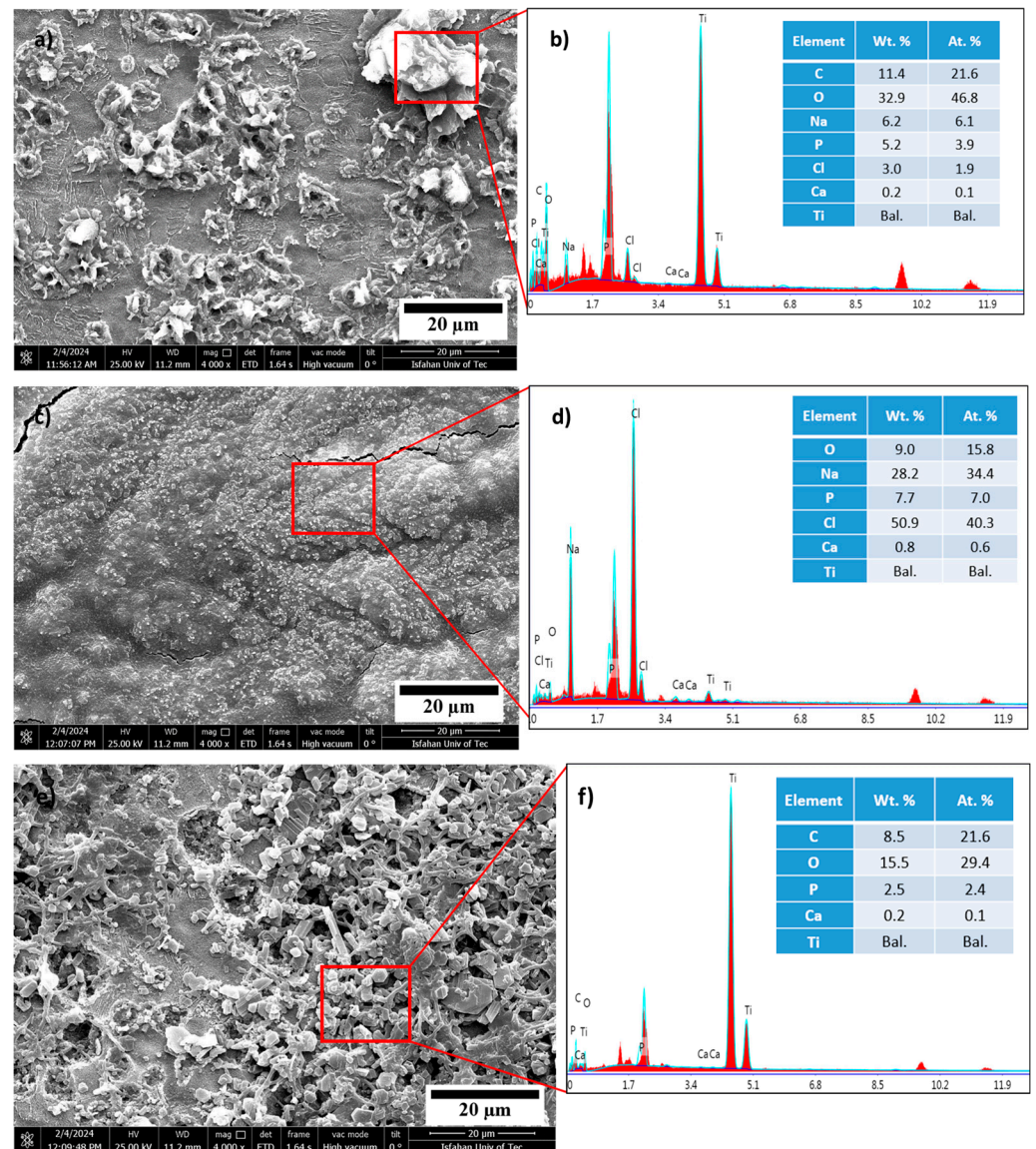
Figure 13. FE-SEM observations for the formation of hydroxyapatite for (**a**,**b**) chitosan, (**c**,**d**) chitosan-1.5% ε-PL, and (**e**,**f**) chitosan-3.0% ε-PL after 2 weeks in the SBF solution.

In orthopedic applications, HA is widely regarded as the gold standard for bioactivity due to its exceptional biocompatibility, ability to promote osteoconduction, and crucial role in the regeneration of damaged bone tissue [46]. The ability of these composite coatings to facilitate HA precipitation, even with some limitations, highlights their potential as promising candidates for further optimization in orthopedic implant technology.

3.10. Degradation Tests

Figure 14 represents the outcomes of the degradation test for chitosan-based layers, showing how different coating layers react with phosphate-buffered saline (PBS) solution (after one week of immersion). Obviously, the presence of ε-PL in the chitosan matrix is associated with a noticeable decrease in the kinetics of degradation. While a complete delamination is observed in the pure chitosan coating layer, the sample chitosan-1.5% ε-PL shows hardly any de-cohesion or delamination, inferring that ε-PL can be seen as an additive that postpones the degradation of the chitosan coating inside the body.
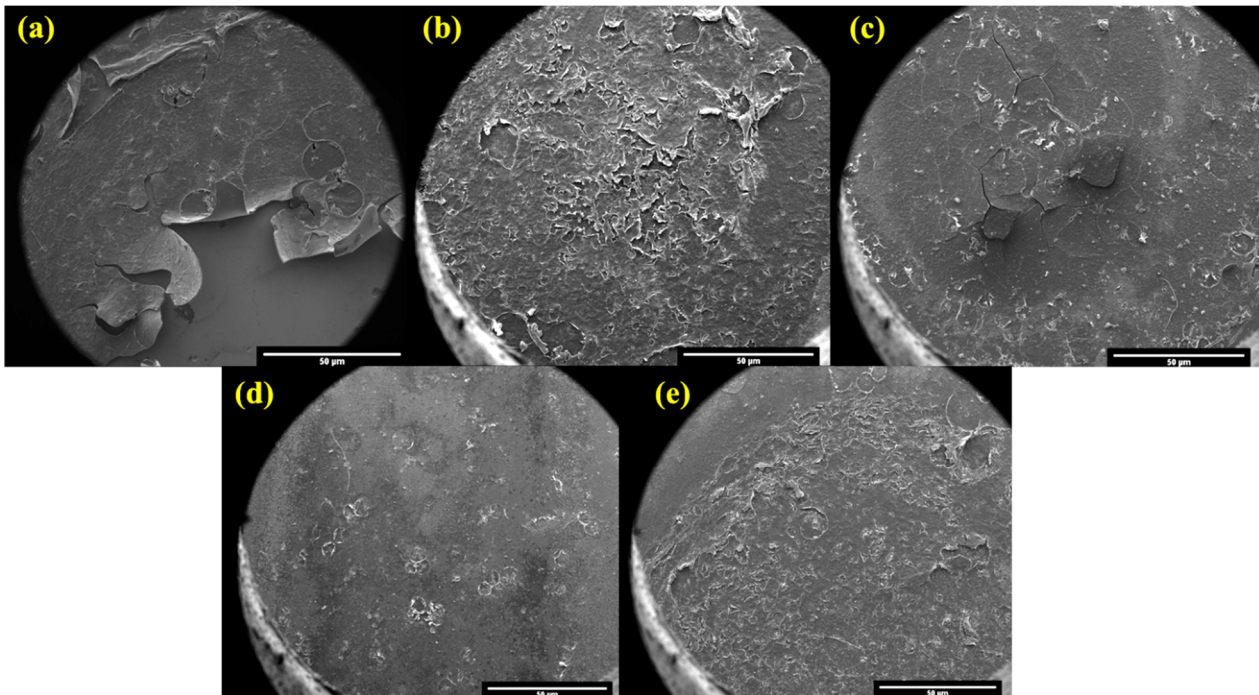
Figure 14. The result of degradation assessment in PBS solution for (**a**) chitosan, (**b**) chitosan-0.5% ε-PL, (**c**) chitosan-1.0% ε-PL, (**d**) chitosan-1.5% ε-PL, and (**e**) chitosan-3.0% ε-PL samples.

4. Conclusions

In this study, the surface modification of anodized titanium surfaces with ε-Polylysine (ε-PL)-containing chitosan coating layers has been investigated. The method involved anodization followed by coating with chitosan, containing different percentages of ε-PL, up to 3 wt.%. Comprehensive analyses using techniques such as XRD, SEM, EDS, and FTIR were carried out to analyze the properties of coating layers. The following conclusions can be drawn from this investigation:

The bioactivity of the composite coatings was assessed through the formation of hydroxyapatite (HA) crystals, a critical indicator of a material's potential in orthopedic applications. Hydroxyapatite, which closely resembles the mineral component of natural bone, plays an essential role in promoting osteoconduction, enhancing biocompatibility, and facilitating bone tissue regeneration. The study demonstrated that the coatings, including chitosan, chitosan-1.5% ε-PL, and chitosan-3.0% ε-PL, were capable of inducing HA precipitation when immersed in simulated body fluid (SBF). This confirms their ability to support mineralization processes relevant for orthopedic use.

SEM/EDS analyses revealed the presence of calcium (Ca) and phosphorus (P) in the precipitated phases across all samples, with evidence of HA formation. However, the relatively low Ca/P ratios indicated moderate bioactivity, suggesting room for optimization to enhance their bone-bonding capacity. Among the samples, chitosan-1.5% ε-PL exhibited the most refined surface morphology, suggesting its potential for improved HA nucleation and growth. This characteristic is particularly advantageous in orthopedic applications, as it can promote better osseointegration and long-term implant stability.

The findings also highlighted that while the addition of ε-PL to the chitosan matrix modified the surface morphology of the precipitated HA, the overall bioactivity was not significantly impacted. Nonetheless, the ability to tailor surface properties and degradation kinetics through ε-PL addition offers a versatile approach for developing coatings with specific orthopedic applications.

Overall, the composite coatings, particularly chitosan-1.5% ε-PL, demonstrate promising potential as candidates for orthopedic implants. Future studies should focus on further

enhancing their bioactivity and evaluating their in vivo performance to confirm their suitability for clinical applications in bone regeneration and implant technologies.

References

1. Xu, Y.; Zhang, F.; Zhai, W.; Cheng, S.; Li, J.; Wang, Y. Unraveling of Advances in 3D-Printed Polymer-Based Bone Scaffolds. *Polymers* **2022**, *14*, 566. [CrossRef] [PubMed]
2. Zhao, Y.; Liu, Y.; Kang, S.; Sun, D.; Liu, Y.; Wang, X.; Lu, L. Peripheral nerve injury repair by electrical stimulation combined with graphene-based scaffolds. *Front. Bioeng. Biotechnol.* **2024**, *12*, 1345163. [CrossRef] [PubMed]
3. Zhang, L.; Shi, H.; Tan, X.; Jiang, Z.; Wang, P.; Qin, J. Ten-gram-scale mechanochemical synthesis of ternary lanthanum coordination polymers for antibacterial and antitumor activities. *Front. Chem.* **2022**, *10*, 898324. [CrossRef] [PubMed]
4. Ras, J.; Leach, L. Relationship Between Physical Activity, Coronary Artery Disease Risk Factors and Musculoskeletal Injuries in the City of Cape Town Fire and Rescue Service. *Inquiry* **2022**, *59*, 00469580221084485. [CrossRef] [PubMed]
5. Coyac, B.R.; Wu, M.; Bahat, D.J.; Wolf, B.J.; Helms, J.A. Biology of sinus floor augmentation with an autograft versus a bone graft substitute in a preclinical in vivo experimental model. *Clin. Oral Implant. Res.* **2021**, *32*, 916–927. [CrossRef] [PubMed]
6. Chen, Z.; Zhang, Z.; Wang, Z.; Wu, J.; Wang, Y.; Si, H.; Xie, X.; Shang, L.; Fan, D.; Chen, F. Fabricating a novel HLC-hBMP2 fusion protein for the treatment of bone defects. *J. Control. Release* **2021**, *329*, 270–285. [CrossRef]
7. Baron, M.; Drohat, P.; Crawford, B.; Hornicek, F.J.; Best, T.M.; Kouroupis, D. Mesenchymal Stem/Stromal Cells: Immunomodulatory and Bone Regeneration Potential after Tumor Excision in Osteosarcoma Patients. *Bioengineering* **2023**, *10*, 1187. [CrossRef]
8. Guo, Y.; Xie, B.; Jiang, M.; Yuan, L.; Jiang, X.; Li, S.; Cai, R.; Chen, J.; Jiang, X.; He, Y.; et al. Facile and eco-friendly fabrication of biocompatible hydrogel containing CuS@Ser NPs with mechanical flexibility and photothermal antibacterial activity to promote infected wound healing. *J. Nanobiotechnol.* **2023**, *21*, 266. [CrossRef]
9. Ong, V.; Soleimani, A.; Amirghasemi, F.; Khazaee Nejad, S.; Abdelmonem, M.; Razaviyayn, M.; Hosseinzadeh, P.; Comai, L.; Mousavi, M.P. Impedimetric Sensing: An Emerging Tool for Combating the COVID-19 Pandemic. *Biosensors* **2023**, *13*, 204. [CrossRef]
10. Watson, E.; Mikos, A.G. Advances in In Vitro and In Vivo Bioreactor-Based Bone Generation for Craniofacial Tissue Engineering. *BME Front.* **2023**, *4*, 0004. [CrossRef]
11. Cakir, F.; Özkal, F.M.; Sensoz, E. Performance Assessment of Biocompatible Metals Used in the Treatment of Femoral Neck Fractures. *ACS Appl. Bio Mater.* **2022**, *5*, 3013–3022. [CrossRef] [PubMed]
12. Abbasi, M.S.; Saber, F.Y.; Bahrami, A.; Torkian, S.; Hosseini-Abari, A. Towards an anticancer bioactive glass-Fe_3O_4/Pectin/Pectic oligosaccharide coatings for biomedical applications. *Surf. Interfaces* **2024**, *45*, 103874. [CrossRef]
13. Heidari Laybidi, F.; Bahrami, A.; Abbasi, M.S.; Rajabinezhad, M.; Heidari Beni, B.; Karampoor, M.R.; Mousavi Anijdan, S.H. Electrophoretic Deposition of ZnO-Containing Bioactive Glass Coatings on AISI 316L Stainless Steel for Biomedical Applications. *Coatings* **2023**, *13*, 1946. [CrossRef]
14. Torkian, N.; Bahrami, A.; Hosseini-Abari, A.; Momeni, M.M.; Abdolkarimi-Mahabadi, M.; Bayat, A.; Hajipour, P.; Rourani, H.A.; Abbasi, M.S.; Torkian, S.; et al. Synthesis and characterization of Ag-ion-exchanged zeolite/TiO_2 nanocomposites for antibacterial applications and photocatalytic degradation of antibiotics. *Environ. Res.* **2022**, *207*, 112157. [CrossRef]
15. Gulati, K.; Ding, C.; Guo, T.; Guo, H.; Yu, H.; Liu, Y. Craniofacial therapy: Advanced local therapies from nano-engineered titanium implants to treat craniofacial conditions. *Int. J. Oral Sci.* **2023**, *15*, 15. [CrossRef]
16. Kiarashi, M.; Mahamed, P.; Ghotbi, N.; Tadayonfard, A.; Nasiri, K.; Kazemi, P.; Badkoobeh, A.; Yasamineh, S.; Joudaki, A. Spotlight on therapeutic efficiency of green synthesis metals and their oxide nanoparticles in periodontitis. *J. Nanobiotechnol.* **2024**, *22*, 21. [CrossRef]
17. Wang, M.; Yao, Q.; Qu, S.; Chen, Y.; Li, H.; Chen, L. Preparation and Thermoelectric Properties of Semiconducting Single-Walled Carbon Nanotubes/Regioregular Poly(3-dodecylthiophene) Composite Films. *Polymers* **2020**, *12*, 2720. [CrossRef]
18. Bispo, M.; Santos, S.B.; Melo, L.D.; Azeredo, J.; van Dijl, J.M. Targeted Antimicrobial Photodynamic Therapy of Biofilm-Embedded and Intracellular Staphylococci with a Phage Endolysin's Cell Binding Domain. *Microbiol. Spectr.* **2022**, *10*, e0146621. [CrossRef]

19. Pihl, M.; Galli, S.; Jimbo, R.; Andersson, M. Osseointegration and antibacterial effect of an antimicrobial peptide releasing mesoporous titania implant. *J. Biomed. Mater. Res. Part B Appl. Biomater.* **2021**, *109*, 1787–1795. [CrossRef] [PubMed]

20. López-Valverde, N.; Aragoneses, J.; López-Valverde, A.; Rodríguez, C.; Macedo de Sousa, B.; Aragoneses, J.M. Role of chitosan in titanium coatings. trends and new generations of coatings. *Front. Bioeng. Biotechnol.* **2022**, *10*, 907589. [CrossRef]

21. Riool, M.; de Breij, A.; Drijfhout, J.W.; Nibbering, P.H.; Zaat, S.A. Antimicrobial peptides in biomedical device manufacturing. *Front. Chem.* **2017**, *5*, 63. [CrossRef] [PubMed]

22. Thambiliyagodage, C.; Jayanetti, M.; Mendis, A.; Ekanayake, G.; Liyanaarachchi, H.; Vigneswaran, S. Recent Advances in Chitosan-Based Applications—A Review. *Materials* **2023**, *16*, 2073. [CrossRef] [PubMed]

23. Qiu, Y.L.; Li, Y.; Zhang, G.L.; Hao, H.; Hou, H.M.; Bi, J. Quaternary-ammonium chitosan, a promising packaging material in the food industry. *Carbohydr. Polym.* **2024**, *323*, 121384. [CrossRef]

24. Zou, Y.; Liu, X.; Chen, Q.; Oku, H.; Ma, G.; Wu, J. Acid-Responsive Immune-Enhancing Chitosan Formulation Capable of Transforming from Particle Stabilization to Polymer Chain Stabilization. *ACS Appl. Mater. Interfaces* **2023**, *15*, 11403–11415. [CrossRef] [PubMed]

25. Yilmaz Atay, H. Antibacterial activity of chitosan-based systems. In *Functional Chitosan*; Springer: Singapore, 2020; pp. 457–489. [CrossRef]

26. Hao, X.; Jiang, B.; Wu, J.; Xiang, D.; Xiong, Z.; Li, C.; Li, Z.; He, S.; Tu, C.; Li, Z. Nanomaterials for bone metastasis. *J. Control. Release* **2024**, *373*, 640–651. [CrossRef]

27. Nie, Y.; Li, D.; Peng, Y.; Wang, S.; Hu, S.; Liu, M.; Ding, J.; Zhou, W. Metal organic framework coated MnO_2 nanosheets delivering doxorubicin and self-activated DNAzyme for chemo-gene combinatorial treatment of cancer. *Int. J. Pharm.* **2020**, *585*, 119513. [CrossRef]

28. Wang, K.; Yin, J.; Chen, J.; Ma, J.; Si, H.; Xia, D. Inhibition of inflammation by berberine: Molecular mechanism and network pharmacology analysis. *Phytomedicine* **2024**, *128*, 155258. [CrossRef]

29. Meissner, J.; Prause, A.; Bharti, B.; Findenegg, G.H. Characterization of protein adsorption onto silica nanoparticles: Influence of pH and ionic strength. *Colloid Polym. Sci.* **2015**, *293*, 3381–3391. [CrossRef]

30. Fernandez-Medina, T.; Vaquette, C.; Gomez-Cerezo, M.N.; Ivanovski, S. Characterization of the Protein Corona of Three Chairside Hemoderivatives on Melt Electrowritten Polycaprolactone Scaffolds. *Int. J. Mol. Sci.* **2023**, *24*, 6162. [CrossRef] [PubMed]

31. Rodrigues, B.; Morais, T.P.; Zaini, P.A.; Campos, C.S.; Almeida-Souza, H.O.; Dandekar, A.M.; Nascimento, R.; Goulart, L.R. Antimicrobial activity of Epsilon-Polylysine against phytopathogenic bacteria. *Sci. Rep.* **2020**, *10*, 11324. [CrossRef] [PubMed]

32. Li, S.; Mao, Y.; Zhang, L.; Wang, M.; Meng, J.; Liu, X.; Bai, Y.; Guo, Y. Recent advances in microbial ε-polylysine fermentation and its diverse applications. *Biotechnol. Biofuels Bioprod.* **2022**, *15*, 65. [CrossRef] [PubMed]

33. Tan, Z.; Shi, Y.; Xing, B.; Hou, Y.; Cui, J.; Jia, S. The antimicrobial effects and mechanism of ε-poly-lysine against *Staphylococcus aureus*. *Bioresour. Bioprocess.* **2019**, *6*, 11. [CrossRef]

34. Alkekhia, D.; Shukla, A. Influence of polylysine molecular weight on antibacterial efficacy in polymer multilayer films. *J. Biomed. Mater. Res. Part A* **2019**, *107*, 1324–1339. [CrossRef]

35. Chen, S.; Huang, S.; Li, Y.; Zhou, C. Recent Advances in Epsilon-Polylysine and L-Lysine-Based Dendrimer Synthesis, Modification, and Biomedical Applications. *Front. Chem.* **2021**, *9*, 659304. [CrossRef]

36. *UNI EN ISO 10993-5:2009*; Biological Evaluation of Medical Devices—Part 5: Tests for In Vitro Cytotoxicity. European Committee for Standardization: Brussel, Belgium, 2009.

37. Bai, M.; Liu, T.; Liu, B.; Li, Y.; Yu, H.; Zhao, Y.; Yang, C.; Song, L.; Liu, W. Preparation and properties of polyurethane cold galvanizing coatings with phosphoric acid modified zinc powder. *Surf. Coat. Technol.* **2024**, *489*, 131128. [CrossRef]

38. Sun, L.; Jiang, Z.; Yuan, B.; Zhi, S.; Zhang, Y.; Li, J.; Wu, A. Ultralight and superhydrophobic perfluorooctyltrimethoxysilane modified biomass carbonaceous aerogel for oil-spill remediation. *Chem. Eng. Res. Des.* **2021**, *174*, 71–78. [CrossRef]

39. Geng, Z.; Chen, C.; Song, M.; Luo, J.; Chen, J.; Li, R.; Zhou, K. High strength $Al_{0.7}CoCrFeNi_{2.4}$ hypereutectic high entropy alloy fabricated by laser powder bed fusion via triple-nanoprecipitation. *J. Mater. Sci. Technol.* **2024**, *187*, 141–155. [CrossRef]

40. Li, S.; Chen, N.; Li, Y.; Li, X.; Zhan, Q.; Ban, J.; Zhao, J.; Hou, X.; Yuan, X. Metal-crosslinked ε-polylysine tissue adhesives with high adhesive performance: Inspiration from mussel adhesive environment. *Int. J. Biol. Macromol.* **2020**, *153*, 1251–1261. [CrossRef]

41. Yang, Q.; Xie, Z.; Hu, J.; Liu, Y. Hyaluronic acid nanofiber mats loaded with antimicrobial peptide towards wound dressing applications. *Mater. Sci. Eng. C* **2021**, *128*, 112319. [CrossRef]

42. Palecek, A.M.; Garner, A.M.; Klittich, M.R.; Stark, A.Y.; Scherger, J.D.; Bernard, C.; Niewiarowski, P.H.; Dhinojwala, A. An investigation of gecko attachment on wet and rough substrates leads to the application of surface roughness power spectral density analysis. *Sci. Rep.* **2022**, *12*, 11556. [CrossRef] [PubMed]

43. Losertová, M.; Štefek, O.; Galajda, M.; Konečná, K.; Martynková, G.S.; Barabaszová, K.Č. Microstructure and Electrochemical Behavior of TiO2 Nanotubes Coated on Titanium-Based Substrate Before and After Thermal Treatment. *J. Nanosci. Nanotechnol.* **2018**, *19*, 2989–2996. [CrossRef] [PubMed]

44. Alinejad-Mofrad, E.; Malaekeh-Nikouei, B.; Gholami, L.; Mousavi, S.H.; Sadeghnia, H.R.; Mohajeri, M.; Darroudi, M.; Oskuee, R.K. Evaluation and comparison of cytotoxicity, genotoxicity, and apoptotic effects of poly-l-lysine/plasmid DNA micro- and nanoparticles. *Hum. Exp. Toxicol.* **2019**, *38*, 983–991. [CrossRef] [PubMed]

45. Hall, A.; Wu, L.P.; Parhamifar, L.; Moghimi, S.M. Moghimi, Differential Modulation of Cellular Bioenergetics by Poly(L-lysine)s of Different Molecular Weights. *Biomacromolecules* **2015**, *16*, 2119–2126. [CrossRef]
46. Abbasi, M.S.; Bahrami, A.; Hosseini-Abari, A.S.; Saber, F.Y. Synthesis and characterization of composite coating of iron oxide and bioactive glass, coated by electrophoretic co-deposition method for biomedical applications. *J. Adv. Mater. Eng.* **2023**, *42*, 1–13.